Author version: Mar. Petrol. Geol., vol.27(10); 2010; 2107-2117

Morphology of pockmarks along the western continental margin of India: employing multibeam bathymetry and backscatter data

Sumanta Dandapath[1], Bishwajit Chakraborty[1,], Siddaiah M. Karisiddaiah[1], Andrew Menezes[1], Govind Ranade[1], William Fernandes[1], Davidas K. Naik[1] and K. N. Prudhvi Raju[2]*

[1]National Institute of Oceanography, Council of Scientific and Industrial Research, Dona Paula, Goa: 403 004, India
[2]Department of Geography, Banaras Hindu University, Varanasi: 221005, India

Abstract

This study addresses the morphology of pockmarks along the western continental margin of India using multibeam bathymetry and backscatter data. Here, for the first time we have utilized the application of ArcGIS (Geographical Information System) for understanding the morphology of pockmarks from the western continental margin of India. The pockmarks observed in water depths of 145-330 m are circular, elliptical or elongated in plan-view, with an average length and width of 157 (±72) m and 83 (±19) m respectively. The average pockmark relief and perimeter are 1.9 (±0.9) m and 412 (±181) m, respectively. The pockmarks have average areas and volumes of 10 759 m² and 15 315 m³ respectively. Spatial separation that coincides with 210 m isobath divides the pockmarks into two groups with differing distributions and morphologies. These pockmarks originated from seepages of biogenic or thermogenic gas or from pore fluids from deeper sources, migrated vertically along the faults. Besides a possible structural control, the pockmark morphologies are also affected by bottom currents and/or by submarine slumping. The average acoustic backscatter strength from pockmark centre is higher (-35 dB) than the average backscatter of the total area (-40 dB), which suggests their possible linkage to the precipitation of diagenitic minerals from biodegradation of seepage material.

Keywords: Pockmark morphology, seafloor seepage, bottom currents, multibeam echo-sounder, backscatter image, continental margin, Arabian Sea

---

* Corresponding author. Tel.: +91 832 2450 318; fax: +91 832 2450 602.

E-mail address: bishwajit@nio.org (B. Chakraborty).

1. Introduction

The presence of fluid escape features like seafloor pockmarks was first introduced by King and MacLean (1970) over the Nova Scotian shelf. Generally, these are either hemispherical or disc shaped seafloor depressions having steep sides and flat floors. Very often, pockmarks exist in the continental margins (Paull et al., 2002; Hovland et al., 2005). In plan-view, these are usually circular, elliptical or elongated, and may be composite in shape. The pockmarks are potentially important for studies of marine resources and environments because of their relationship with venting of gas or other fluids generated by biogenic or thermogenic processes (Floodgate and Judd, 1992; Judd and Hovland, 2007; Rollet et al., 2009). Multibeam echo-sounders are potentially useful for locating and mapping these pockmarks (Rollet et al., 2006; Chand et al., 2009). Kelley et al. (1994) suggest two models for pockmark formation namely, i) an equilibrium model, wherein pockmarks are thought to have been formed slowly over thousands of years, and ii) a catastrophic model, for pockmarks that might have been formed during an earthquake, tsunami and/or a storm, with large quantities of muddy sediments being transported during the formation. Recently, Cathles et al. (2010) demonstrated a different model of gas induced pockmark formation: a) gas trapped below a capillary seal of fine grained sediments, b) increasing gas accumulation causing failure of seals and formation of upward moving gas chimney dislocating pore waters, c) surface deformation initiated and quickened sediments removed by bottom currents causing formation of pockmarks.

Pockmark size, shape and spatial distribution reflect the capacity and composition of fluid reservoirs sourcing the venting fluids (Hovland and Judd, 1988; Hovland et al., 2002; Pilcher and Argent, 2007), type of the fluid escape (Bøe et al., 1998), sediment characteristics and configuration of underlying structures (Gay et al., 2006), water depth and morphology of the surrounding seafloor. Faults and fractures provide permeability conduits for fluids or gas migrating to the surface (Boever et al., 2009). A typical dimension for shallow water (shelf) pockmarks are 40-150 m wide, 60-200 m long, and 2-10 m vertical relief, though globally they can vary between 10-300 m in width, 20-1000 m in length and up to 45 m in relief (Pilcher and Argent, 2007; Andresen et al., 2008).

Marine geophysical studies of the western continental margin of India (WCMI) have revealed that, the presence of surficial and sub-surficial geology relates to in-situ gas and its seepage (prominently methane), including gas-charged sediments and “V” shaped depressions (Karisiddaiah and

Veerayya, 1994; Karisiddaiah et al., 2002; Karisiddaiah and Veerayya, 2002), diapirs (Satyavani et al., 2005) and Bottom Simulating Reflectors (BSRs; Veerayya et al., 1998; Rao et al., 1998, 2001; Satyavani et al., 2005, Dewangan and Ramprasad, 2007). Present study, documents comprehensive pockmark morphology of the WCMI area (Fig. 1a and b) based on the multibeam bathymetry and backscatter data with an emphasis on their processes of formation. Additional supporting shallow seismic and single-beam echo-sounder data were also utilized for the validation of pockmarks in order to justify their association with possible migration pathways.

2. Regional setting

A number of deep seated faults, reefs, basement highs, and ridge systems have been identified along the WCMI (Bhattacharya and Chaubey, 2001). The general orientation of these structural features is NNW-SSE and parallel to the coast. The faults in this region are also parallel to the Dharwar Precambrian orogenic trend (Biswas, 1987). The shape of the continental margin having wider shelf (345 km) and narrow slope in the north compared to a narrow shelf (60 km) and wider slope in the south is conspicuous (Veerayya et al., 1991). Reineck and Singh (1980) concluded that the upper slope region being adjacent to shelf break/edge experiences complex hydrodynamic environment, which also affects sedimentological regime.

Present study area stretches over 105 km² offshore Goa along WCMI (Fig. 1a and b), in water depths ranging from 145 m in the northeast to 330 m in the southwest. The average slope of the study area is 0.90˚, whereas the slope towards the shallower depth is 0.61˚, and towards the deeper side this slope changes over to 1.68˚. Rao and Rao (1995) have reported that the recent clay-rich mud overlies the inner part of this slope area while relict sand is abundant in the outer slope area. In this work, using multibeam data, set of pockmarks were observed close to NNW-SSE trending fault zone (Fig. 1b). The margin is believed to have been formed in two phases in geological past (Mukhopadhyay et al., 2008). Interestingly, these pockmarks (totaling 112) are observed nearly 50 km away from a BSR zone (Rao et al., 2001) marked in Fig. 1a. A strong coast parallel (NNW-SSE trending) bottom current covering 40 km wide runs through the present study area (Shetye et al., 1990) (Fig. 1b).

3. Methods

The survey was conducted in 2006 onboard the Coastal Research Vessel (CRV) *Sagar Sukti* employing Kongsberg EM1002 multibeam echo-sounder operating at a frequency of 95 kHz. The backscatter data is provided by the multibeam sonar as seafloor backscatter strength, which is a quantitative measure of the proportion of the sound incident on the seafloor that is scattered back towards the sonar. The backscatter data is corrected for propagation and other effects (Mitchell and Somers, 1989). The backscatter data are post processed using Neptune (developed by Kongsberg Simrad) and CFLOOR (developed by Cfloor AS) software for improved visualization including tide correction and gridding (grid resolution: 10 x 10 m; Fernandes and Chakraborty, 2009). Backscatter strengths shown here are mean values, having been filtered by the sonar to provide beam-averages and then spatially averaged in our gridding procedure, hence they lack speckle observed in raw side-scan sonar images (Mitchell, 1991). For the first time from the western continental margin of India a detailed morphology of 112 pockmarks-like features were studied with the help of ArcGIS (Geographical Information System) developed by ESRI Inc., USA. Spatial analyst extension (a separate module added with ArcGIS) was also used for raster based spatial analyses of data. All the measurements were done using ArcGIS tools.

4. Observations

4.1. Pockmark morphology and spatial distribution

In this section we have presented pockmark morphological parameters using multibeam bathymetry data and GIS. Combined observation of bathymetry and backscatter data enabled us to assess and estimate the morphological parameters of the pockmarks. We have detected a total of 112 pockmarks of which 43 are circular, 51 are elliptical and remaining 18 are of elongated type. A brief account of dimensions, shape, cross-section, orientations, and spatial distribution of the pockmarks is given below:

Most pockmarks are small to medium sized, with lengths varying from 70 m to 514 m (Fig. 2a) and widths from 50 m to 136 m (Fig. 2b). The average length and width are 157 m and 83 m, respectively. Pockmark vertical relief varies from 0.7 m to 5.0 m (Fig. 2c) with an average of 1.9 m. In addition, there are 11 and 16 pockmarks of relief >3 m and <1 m respectively. The distance around each

pockmark perimeter varies between 200 m and 1225 m with an average of 412 m (Fig. 2d). From the Fig. 2a-d we observed that all the measured parameters (i.e., length, width, relief and perimeter) of the pockmarks appear to be unimodal in distribution. However, for length, relief and perimeter the graph is positively skewed, which is not the case for width. Standard deviation (SD) for length (±72 m), relief (±0.9 m) and perimeter (±181 m) is also much higher than the width (±19 m). The average pockmark surface area is 10 759 m² and it ranges in between 2914 m² – 33 507 m². Collectively they cover a cumulative area of 1.20 km² representing 1.1% of the total study area. However, in the deeper area (beyond the 210m water depth) it covers as much as 10% seafloor area close to the fault zone (area ~5 km^2) (Fig. 1b). In contrast to our study, the reported values of nearly or less than 5% at North Sea (Judd and Hovland, 2007) and 7.7% at Penobscot Bay region (Gontz, 2002) are quite interesting. Volume of the pockmarks which ranges from 1620 m^3 to 76 538 m^3 with an average of 15 315 m^3 indicates over 1.72 x 10^6 m^3 sediment from ~105 km^2 area has been excavated in the processes later related to the pockmark formation. This estimated value differs from the reported ones observed elsewhere [higher than the northern California region (6.6 x 10^5 m^3 from ~2100 km^2 area; Yun et al., 1999), and lower than the Penobscot Bay region (2.10 x 10^6 m^3 from 38 km^2 area; Gontz et al., 2002)].

In plan-view, pockmarks are generally circular (L/W = 1.0-1.5; 38%; Fig. 3a), or elliptical (L/W = 1.5-2.5; 46%; Fig. 3b), and also elongated in shape (L/W = ≥2.5; 16%; Fig. 3c). The plan-view aspect ratio (length/width) ranges from 1.03 to 6.19 and positively skewed with a mean of 1.90 (Fig. 2e). Elliptical and elongated pockmarks merge each other in order to form complex shapes (Fig. 3d-f). The geometry of the majority pockmarks in cross-sections (Fig. 4a-c) are mainly 'V'-shaped (more than 60%), while remaining are 'U'- and 'W'-shaped. Along the continental slope region, sidewall heights of the pockmarks between the up- and down-slope sides vary up to 6 m. Again, average slope angle of the sidewall varies between 0.90˚ and 5.06˚ for individual pockmarks (Fig. 2f) with a mean value of 2.51˚ (SD ±0.9˚). In this area, most of the large-sized pockmarks (relief >3 m) have a greater slope angle (slope >3˚) compared to the smaller one. Pockmark clusters and chains are observed along with randomly distributed ones. Nearly one-third of the pockmarks are asymmetric in profile.

The orientation of the pockmark major axis (length) was measured and analyzed to interpret the influence of underlying structure and other processes. Fig. 5a shows the orientations as a rose diagram, illustrating the tendency of the pockmarks to be aligned around NNW-SSE direction. Of the elongated

pockmarks, 44% are oriented NNW-SSE and 33% are oriented N-S direction (Fig. 5b). The trend of the pockmark orientation follows both the fault and bottom current directions (Fig. 1b).

The depths over which pockmarks are found vary from 168 m in the east to 282 m in the west (Figs. 1b and 5c). The 210 m isobath shown in Fig. 1b separates the area into two distinct zones with differing distributions and morphologies of pockmarks. In the deeper water near the fault, pockmark density is high (5-6/km²) and they occur in a linear band parallel with the fault. Most of the pockmarks (nearly 80%) in the deeper slope region constitute a band of linear chains. Towards the shallow region, pockmarks are quasi-randomly distributed.

Three dimensional multibeam bathymetry data also show deep water pockmarks, which are frequently associated with the NNW-SSE trending faults (Fig. 6a). A stretch of 5.0 km long single-beam echo-sounder (frequency: 33 kHz) section (referred to as line AB in Fig 6b) obtained within this area reveals two faults, presence of a pockmark (approximate dimensions: 4 m deep, 120m wide) and seeps (at 235 and 255 m water depths). A terrace like feature detected at 210m water depth (Fig 6b).

Besides, we have also presented eight kilometer long single channel sparker (4.5 kJ) profile (Fig. 7a) marked as SW-NE in the multibeam three dimensional map (Fig. 6a). Sub-bottom profiler (frequency: 3.5 kHz) data (Fig. 7b) along with the multibeam bathymetry (Fig 7c) and backscatter (Fig. 7d) data are also given. Analyses of sparker data reveal the presence of three pockmarks (P), three shallow faults (F), and five distinguishing reflectors. Interestingly, the backscatter data (Fig 7d) does show a buried pockmark (Bp) which is also seen as a blurred object in the high resolution seismic profile (Fig. 7a).

4.2. Backscatter characteristics

Acoustic backscatter strength of the area ranges from -26 to -57 dB (Fig. 1b). Such backscatter variability is related to the seafloor slope, sediment type and relief (Blondel and Murton, 1997). Fig. 5d shows backscattering strength at different water depths for each individual pockmark centre. In the deeper water (>210 m), many pockmarks show high backscatters centrally (-27 to -40 dB). Towards the west in deeper water, the seafloor has strong backscatter (-35 dB) suggesting coarser grained sediment at the seafloor because of increased acoustic impedance (Wen and Larsen, 1996) and roughness-related scattering from coarse sediment (Goff et al., 2000). In shallow water (<210 m) where seabed gradients

are gentle, normally backscatter strength is low. The area is covered by soft terrigenous clayey mud producing average seafloor backscatter strength (-45 dB). Occasional discrete curvilinear, circular or clustered patches of higher backscatter (-32 dB) occur towards the shallower part (Fig. 1b). Strong backscatter (-30 to -38 dB) is also observed around the fault. The variation in backscatter observed between these different areas is broadly comparable with results of calibrated acoustical measurements between different known sediment types (e.g., Urick, 1983).

5. Discussion

5.1. Origin of the pockmarks

The presence of gas-charged sediments along the continental margin of the eastern Arabian Sea has been reported by Karisiddaiah and Veerayya (1994). Conspicuous BSRs (Fig. 1a) have also been reported in seismic reflection data from middle and lower slope region (Veerayya et al., 1998; Rao et al., 1998, 2001; Satyavani et al., 2005; Dewangan and Ramprasad, 2007), which might be associated with gas hydrates. In the present study area, deep sediment cover, higher proportion of hydrogen-rich (marine origin) organic carbon (Paropkari et al., 1993), and its good preservation by a permanent oxygen-minimum zone create ideal conditions for the generation of hydrocarbon in the subsurface sediments. Diapir-like features in the BSRs and substantial seismic evidence of methane in the deeper water supports the existence of methane beneath the seafloor in this area (Satyavani et al., 2005). Multibeam bathymetry and a single-beam echo-sounder section (Fig. 6) and high resolution single channel sparker section along with corresponding sub-bottom profiler, multibeam bathymetry and backscatter profile (Fig. 7) helps us to locate three distinct faults and their close association with the pockmarks in the study area including two possible seeps. These shallow faults are possibly linked to either i) BSR zone in the slope region or ii) the subsurface reservoir of hydrocarbon bearing sediments in the deep, and thus might have carried the fluid to the surface leading to the formation of pockmarks. The reactivation of existing faults directly or indirectly may have played a key role in developing these pockmarks at different geological time. We presume that in the shallower part certain high backscatter patches (indicated in Fig. 1b and 7d) resemble buried pockmarks (Bp), which may be similar to the ones reported by Karisiddaiah and Veerayya (2002). We conclude that the fluid/gas might have been generated either from biogenic or thermogenic processes as explained elsewhere (e.g., Floodgate and Judd, 1992).

5.2. Morphological modifications

Gas escape and erosion from a point source into unconsolidated sediment will produce circular depressions (Hovland et al., 2002). The elliptical and elongated pockmarks in the fault area may have initially been circular but were later modified by bottom currents and/or by coalescing with each other due to submarine slumping.

5.2.1. Bottom currents and pockmark morphology

Shetye et al. (1990) have reported the existence of a 40 km wide bottom currents over the WCMI based on hydrographic observations. The bottom currents move northward carrying low salinity water during southwest monsoon and move southward carrying high salinity water during northeast monsoon. In the study area, bottom currents (~250 m) are parallel to the bathymetric contours and are similar to the orientation of the pockmarks (rose diagram in Fig. 5a). This suggests the possibility of bottom currents actively participating in modifying the pockmark shape. Pockmarks either may be eroded by scouring bottom currents are getting larger and elongated along the direction of bottom currents or the currents themselves prevent the deposition of sediments over the pockmarks. Presence of buried pockmarks may indicate higher sediment deposition over the pockmarks which may be due to weaker strengths or absence of the bottom currents. Occurrence of >30% elongated (L/W = ≥2.50) pockmarks in the shallower depth (<210 m) as compared to 10% in the deeper areas (>210 m) indicates to have higher impact of bottom currents in the shallower part than in the deeper area. It is also possible that the shallow water pockmarks (i.e., located some distance from faults) might have been formed much before the deeper ones (near the faults) and thus bottom currents were involved in the modification process for a much longer time. Hovland et al. (2002) have demonstrated the strength of bottom currents in modifying the shape of pockmarks. Current-controlled pockmarks as noticed in the present study area along WCMI, were also reported elsewhere, e.g., in the Skagerrak and North Sea region (Bøe et al., 1998; Andresen et al., 2008).

5.2.2. Faults and pockmark morphology

Pockmarks are often observed along fault strike on the seafloor. This is better explained by the development of weaker lithospheric stress along the fault trace which usually acts as a vertical migration path for fluid expulsion from deeper sources to the seafloor. Besides their substantial impact on origin

(discussed in section 5.1), faults also have played a major role in shaping the morphological evolution of these pockmarks. As mentioned earlier, the bimodal distribution in the Fig. 8 is also affirmed that the pockmarks in the area are possibly formed in two different phases in the geological past. Therefore, they are concentrated in two different regions i.e., a) over and around the central fault, and b) in the shallow area, 2-6.5 km distance from central fault. At depths between 228-240 m, pockmarks are normally observed along the strike of a fault running NNW-SSE direction (Figs. 1b and 6a). Pockmarks located along this fault zone are commonly elliptical in shape and having similar orientation of bottom currents and faults (i.e., NNW-SSE). We could also find progressive development of pockmarks (from 'V'- to 'U'- and then 'W'- shape) and formation of pockmark chain (Fig. 3e and f) along the fault-strike which is somehow similar to the pockmark 'gully' observed off-Gabon continental margin (Pilcher and Argent, 2007). Due to the conditions like similar orientation of bottom currents with the fault axis, and faults acting as migration pathways of fluid/gas, the pockmark chain observed under study might have been formed only above the fault axis.

5.2.3. Submarine slumping and pockmark morphology

Submarine slumping along the WCMI is reported by Rao (1989) and Guptha et al. (2002) particularly on the upper slope. Guptha et al. (2002) suggested an episodic slumping during different geological periods triggered by gravity, earthquake, and storm surges. They also proposed evolution of methane as a possible reason for slumping along WCMI during the Holocene. Thus, presence of pockmarks in the region and their detailed morphological characteristics (e.g., shape, sidewall slope etc.) had strengthened such possibilities. We speculate that uprising gas bubbles and gravitational pulls along the sidewall of the pockmarks might have initiated slumping. Similar events due to upward migration of gas were also recorded from the eastern Black Sea region (Ergün et al., 2002) and US Atlantic continental slope (Carpenter, 1981). The correlation between average slope angle of sidewall and relief of pockmarks (Fig. 9a) is very strong ($r = 0.86$), which points to an unstable seafloor around pockmarks. Frequent association of larger pockmarks and steeper slope exhibit the progressive pressure building around the pockmarks. Considering the gradual increase of steepness of the seafloor towards the deeper side especially after 210 m depth, it is expected to have higher gravitational pull for the deeper water pockmarks than those located in shallow water. Maximum occurrence of composite pockmarks (which is supposed to be developed due to collapse of their common sidewalls) in the deeper area especially above the fault is evident of slumping in this region. It is also worth mentioning that the 'W'-shape

pockmarks even above the fault-strike may have been formed by coalescing with each other due to slumping as the fault zone is also represented by weaker lithospheric strength and therefore highly susceptible for slumping. Çifçi et al. (2003) concluded that elongated pockmarks may form by merging of the smaller size circular pockmarks perpendicular to the slope direction and along the linear weakness zone due to down-slope stretching behind the shelf break. They had also observed similar unstable sidewalls of the pockmarks. Despite this we believe that the impact of bottom currents and faults is much stronger than that of submarine slumping to modify pockmark morphology in the study area.

5.3. Pockmark morphologic characteristics

We have attempted correlation studies to substantiate the variations in pockmark shape (Fig. 9b-d). Pockmark length is moderately correlated with relief ($r = 0.42$; Fig. 9b). Separating the population into two groups according to water depth, those deeper than 210 m have $r = 0.62$ whereas those shallower than 210 m have $r = 0.48$. Pockmark width is more strongly correlated with relief ($r = 0.62$; Fig. 9c). Again splitting the population into two groups, the deeper water data have $r = 0.70$ compared with only $r = 0.27$ for the shallower water depths. Similar statements can be made for pockmark perimeters (Fig. 9d). The somewhat greater correlations for the deeper water pockmarks indicate limited modification of pockmark morphology. Furthermore, when correlating morphological parameters, we could find a transition at around 1.5-2 m relief for length (Fig. 9b) and perimeter (Fig. 9d) but not in terms of width (Fig. 9c). This trend point towards a progressive development of the morphology by growth of isolated initially sub-circular pockmark, originally occurring in groups aligned with the fault. If pockmarks initially started off being elongated it would not have exhibited the same trend. From present study we cannot rule out the possibilities of presence of unit-pockmarks (<5 m diameter) as described by Hovland et al. (2010) using ROV based sonar system. However, in this study we have employed high resolution multibeam system installed onboard, which could only detect medium sized pockmarks at the water depths of 145 to 330 m.

5.4. Backscatter variability in relation to pockmarks

We have visualized an abrupt increase in backscatter strength of 5-10 dB around the pockmark depressions (see Fig. 4a-c), and is also significantly higher within the pockmark-dominated areas, as reported elsewhere (Sahling et al., 2008a; Naudts et al., 2008). The variability of backscatter strength of the pockmarks is also affected by slope, sediment type and relief of the seafloor. Average backscatter

strength in the deeper area (-35 dB) is higher compared to the shallower area (-45 dB) due to different acoustic impedance and roughness related scattering. High seafloor backscatter in the deeper pockmark zone is attributed to coarse sediment, which might have been left inside the pockmarks due to winnowing of fine-grained sediments (Çifçi et al., 2003). Likewise, the coarse fraction could also result from the precipitation of diagenitic or authigenic minerals associated with fluid venting (Sahling et al., 2008b; Feng et al., 2009). Low backscatter strengths in the shallower areas are caused by different types of recent sediments (clays). In such areas, however, occasional high backscatter patches surrounded by low backscatter ones are associated with sediment movement as observed elsewhere (Naudts et al., 2008). Although, the backscatter over the whole study area varies widely from -26 to -57 dB, but within the pockmark itself, it is limited (-27 to -48 dB; Fig. 5d) and much higher (Ergün et al., 2002; Çifçi et al., 2003; Chand et al., 2009).

6. Conclusions

In this communication extensive application of GIS for detailed pockmark morphology is being carried out for the first time. The pockmarks under study were mainly noticed in the deeper area and appear strongly associated with fault and potentially with the fluid escape in the form of seep to the surface. Existing fault zone is considered to be linked with the BSRs located in the slope region or to the deep hydrocarbon reservoirs, and carry the gas/fluid to the surface leading to the formation of pockmarks in the region that later modified by combined effects of bottom currents and submarine slumping. Occasional formation of pockmark chain above the fault axis is worth mentioning. Our study, demonstrates that nearly 1.72 x 10^6 m^3 sediment from ~105 km^2 area excavated during the processes of pockmark formation.

The study of pockmark shapes and orientation shows that the deep water pockmarks are generally elliptical and are controlled by faults, bottom currents and slumping. Conversely elongated shallow water pockmarks (i.e., some distance from the fault) appear to be due to sediment transport driven by the bottom currents. During the various sedimentation processes, the effect of bottom or contour currents was considered as one of the important aspects for the modification of pockmarks.

Variable backscatter strengths from the present study area reveal varying sedimentological changes on either side of the 210 m isobath. High backscatter in the deeper pockmark zone suggests generally coarser sediment, possibly linked to the precipitation of diagenitic minerals from

biodegradation of seepage material. Generally low but varied backscatter strength in the shallower area is associated with seafloor inhomogeneity due to sediment movements over a clayey surface.

In this attempt we have studied pockmark dimension using onboard installed multibeam system, however, in future we planned to employ ROV based sonar to identify the smaller sized pockmarks of <5 m diameter as reported by Hovland et al. (2010).

Acknowledgements

We sincerely acknowledge Dr. S. R. Shetye, Director, NIO, for permission to carry out this work. The multibeam data was acquired under the Exclusive Economic Zone mapping program (GAP 1438/2002) of the Ministry of Earth Sciences, New Delhi and backscatter processing was carried out under National Institute of Ocean Technology (NIOT), Chennai funded project (GAP 2248). We express gratitude to Dr. Neil C. Mitchell, University of Manchester, UK for his thoughtful and constructive comments. We also place on record the dedicated efforts of the associate editor Dr. Finn Surlyk and two anonymous reviewers whose thoughtful suggestions considerably improved the contents of the original manuscript. One of the authors (SD) acknowledges financial support from a CSIR NET fellowship. This is NIO contribution no. xxxx.

References

Andresen, K.J., Huuse, M., Clausen, O.R., 2008. Morphology and distribution of Oligocene and Miocene pockmarks in the Danish North Sea – implications for bottom current activity and fluid migration. Basin Res. 20, 445-466.

Bhattacharya, G.C., Chaubey, A.K., 2001. Western Indian Ocean – A Glimpse of the Tectonic Scenario. In: Gupta R.S., Desa, E. (Ed.), The Indian Ocean – A Perspective. Oxford-IBH, New Delhi, pp. 691-729.

Biswas, S.K., 1987. Regional tectonic framework, structure and evolution of the western marginal basins of India. Tectonophysics 135, 307-327.

Blondel, P., and Murton, B.J., 1997. Handbook of Seafloor Sonar Imagery. Wiley-Praxis Series in Remote Sensing. John Wiley and Sons Ltd., Chichester, 314pp.

Boever, E.D., Huysmans, M., Muchez, P., Dimitrov, L., Swennen, R., 2009. Controlling factors on the morphology and spatial distribution of methane-related tubular concretions – Case study of an Early Eocene seep system. Mar. Petrol. Geol. 26, 1580-1591.

Bøe, R., Rise, L., Ottesen, D., 1998. Elongate depressions on the southern slope of the Norwegian Trench (Skagerrak): morphology and evolution. Mar. Geol. 146, 191-203.

Carpenter, G., 1981.Coincident sediment slump/clathrate complexes on the U.S. Atlantic continental slope. Geo-Mar. Lett. 1, 29-32.

Cathles, L.M., Su, Z., Chen, D., 2010. The physics of gas chimney and pockmark formation, with implications for assessment of seafloor hazards and gas sequestration. Mar. Petrol. Geol. 27, 82-91.

Chand, S., Rise, L., Ottesen, D., Dolan, M.F.J., Bellec, V., Bøe, R., 2009. Pockmark-like depressions near the Goliat hydrocarbon field, Barents Sea: morphology and genesis. Mar. Petrol. Geol. 26, 1035-1042.

Çifçi, G., Dondurur, D., Ergün, M., 2003. Deep and shallow structures of large pockmarks in the Turkish Shelf, Eastern Black Sea. Geo-Mar. Lett. 23, 311-322.

Dewangan, P., Ramprasad, T., 2007. Velocity and AVO analysis for the investigation of gas hydrate along a profile in the western continental margin of India. Mar. Geophys. Res. 28, 201-211.

Ergün, M., Dondurur, D., Çifçi, G., 2002. Acoustic evidence for shallow gas accumulations in the sediments of the eastern Black Sea. Terra Nova 14, 313-320.

Feng, D., Chen, D., Peckmann, J., Bohrmann, G., 2010. Authigenic carbonates from methane seeps of the northern Congo fan: Microbial formation mechanism. Mar. Petrol. Geol. 27, 748-756.

Fernandes, W., Chakraborty, B., 2009. Multi-beam backscatter image data processing techniques employed to EM 1002 system. IEEE OES Proceedings of the International Symposium on Ocean Electronics (SYMPOL 2009). Department of Electronics, Cochin University of Science and Technology, Kochi, India, pp. 93-99.

Floodgate, G.D., Judd, A.G., 1992. The origin of shallow gas. Cont. Shelf Res. 12, 1145-1156.

Gay, A., Lopez, M., Cochonat, P., Seranne, M., Levache, D., Sermondadaz, G., 2006. Isolated seafloor pockmarks linked to BSRs, fluid chimneys, polygonal faults and stacked Oligocene-Miocene turbiditic paleochannels in the Lower Congo Basin. Mar. Geol. 226, 25-40.

Goff, J.A., Olson, H.C., Duncan, C.S., 2000. Correlation of side-scan backscatter intensity with grain-size distribution of shelf sediments, New Jersey margin. Geo-Mar. Lett. 20, 43-49.

Gontz, A.M., 2002. Evolution of seabed pockmarks in Penobscot Bay, Maine. MS Thesis, University of Maine, Orono, 118pp.

Gontz, A.M., Belknap, D.F., Kelley, J.T., 2002. Seafloor features and characteristics of the Black Ledges area, Penobscot Bay, Maine, USA. J. Coast. Res. S1 36, 333-339.

Guptha, M.V.S., Mohan, R., Muralinath, A.S., 2002. Slumping on the western continental margin of India. GeoActa 1, 45-48.

Hovland, M., Judd, A.G., 1988. Seabed Pockmarks and Seepages – Impact on Geology, Biology and the Marine Environment. Graham & Trotman, London, 293pp.

Hovland M., Gardner J.V., Judd, A.G., 2002. The significance of pockmarks to understanding fluid flow processes and geohazards. Geofluids 2, 127-136.

Hovland, M., Svensen, H., Forsberg, C.F., Johansen, H., Fichler, C., Fosså, J.H., Jonsson, R., Rueslåtten, H., 2005. Complex pockmarks with carbonate-ridges off mid-Norway: Products of sediment degassing. Mar. Geol. 218, 191-206.

Hovland, M., Reggland, R., De Vries, M.H., Tjelta, T.I., 2010. Unit-pockmarks and their potential significance for predicting fluid flow. Mar. Petrol. Geol. 27, 1190-1199.

Judd, A., Hovland, M., 2007. Seabed Fluid Flow – The Impact on Geology, Biology and the Marine Environment. Cambridge University Press, NewYork, 475pp.

Karisiddaiah, S.M., Veerayya M., 1994. Methane-bearing shallow gas-charged sediments in the eastern Arabian Sea: a probable source for greenhouse gas. Cont. Shelf Res. 14, 1361-70.

Karisiddaiah, S.M., Veerayya, M., 2002. Occurrence of pockmarks and gas seepages along the central western continental margin of India. Curr. Sci. 82, 52-57.

Karisiddaiah, S.M., Veerayya, M., Vora, K.H., 2002. Seismic and sequence stratigraphy of the central western continental margin of India: late-Quaternary evolution. Mar. Geol. 192, 335-353.

Kelley, J.T., Dickson, S.M., Belknap, D.F., Barnhardt, W.A., Henderson, M., 1994. Giant sea-bed pockmarks: evidence for gas escape from Belfast Bay, Maine. Geology 22, 59-62.

King, L.H., MacLean, B., 1970. Pockmarks on the Scotian Shelf. Geol. Soc. Am. Bull. 81, 3141-3148.

Mitchell, N.C., and Somers, M.L., 1989. Quantitative backscatter measurements with long range side-scan sonar. IEEE J. Oceanic Eng. 14, 368-374.

Mitchell, N.C., 1991. Improving GLORIA images using Sea Beam data. J. Geophys. Res. 96, 337-351.

Mukhopadhyay, R., Rajesh, M., De, S., Chakraborty, B., Jauhari, P., 2008. Structural highs on the western continental slope of India: Implications for regional tectonics. Geomorphology 96, 48-61.

Naudts, L., Greinert, J., Artemov, Y., Beaubien, S.E., Borowski, C., Batist, M.D., 2008. Anomalous sea-floor backscatter patterns in methane venting areas, Dnepr paleo-delta, NW Black Sea. Mar. Geol. 251, 253-267.

Paropkari, A.L., Babu, C.P., Mascarenhas, A., 1993. New evidence for enhanced preservation of organic carbon in contact with oxygen minimum zone on the western continental slope of India. Mar. Geol. 111, 7-13.

Paull, C., Ussler III, W., Maher, N., Greene, H.G., Rehder, G., Lorenson, T., Lee, H., 2002. Pockmarks of Big Sur, California. Mar. Geol. 181, 323-335.

Pilcher, R., Argent, J., 2007. Mega-pockmarks and linear pockmark trains on the West African continental margin. Mar. Geol. 244, 15-32.

Rao, P.S., 1989. Ooid turbidites from the central western continental margin of India. Geo-Mar. Lett. 9, 85-90.

Rao, V.P., Rao, B.R., 1995. Provenance and distribution of clay minerals in the sediments of the western continental shelf and slope of India. Cont. Shelf Res. 15, 1757-1771.

Rao, Y.H., Reddi, S.I., Khanna, R., Rao, T.G., Thakur, N.K., Subrahmanyam, C., 1998. Potential distribution of methane hydrates along the Indian continental margins. Curr. Sci. 74, 466-468.

Rao, Y.H., Subrahmanyam, C., Rastogi, A., Deka, B., 2001. Anomalous features related to Gas/Gas hydrate occurrences along the western continental margins of India. Geo-Mar. Lett. 21, 1-8.

Reineck, H.-E., Singh, I.B., 1980. Depositional Sedimentary Environments, second ed. Springer-Verlag, Berlin. 549pp.

Rollet, N., Logan, G.A., Kennard, J.M., O'Brien, P.E., Jones, A.T., Sexton, M., 2006. Characterisation and correlation of active hydrocarbon seepage using geophysical data sets: An example from the tropical, carbonate Yampi Shelf, Northwest Australia. Mar. Petrol. Geol. 23, 145-164.

Rollet, N., Logan, G.A., Ryan, G., Judd, A.G., Totterdell, J.M., Glenn, K., Jones, A.T., Kroh, F., Struckmeyer, H.I.M., Kennard, J.M., Earla, K.L., 2009. Shallow gas and fluid migration in the northern Arafura Sea (offshore Northern Australia). Mar. Petrol. Geol. 26, 129-147.

Sahling, H., Bohrmann, G., Spiess, V., Bialas, J., Breitzke, M., Ivanov, M., Kasten, S., Krastel, S., Schneider, R., 2008a. Pockmarks in the Northern Congo Fan area, SW Africa: Complex features shaped by fluid flow. Mar. Geol. 249, 206-225.

Sahling, H., Mason, D.G., Ranero, C.R., Huchnerbach, V., Weinrebe, W., Klaucke, I., Buerk, D., Brueckman, D., Suess, E., 2008b. Fluid seepage at the continental margin offshore Costa Rica and Southern Nicargua. Geochem. Geophys. Geosyst. 9, 1-22.

Satyavani, N., Thakur, N.K., Aravind Kumar, N., Reddi, S.I., 2005. Migration of methane at the diapiric structure of the western continental margin of India – insights from seismic data. Mar. Geol. 219, 19-25.

Shetye, S.R., Gouveia, A.D., Shenoi, S.S.C., Sundar, D., Michael, G.S., Almeida, A.M., Santanam, K., 1990. Hydrography and circulation off the west coast of India during the southwest monsoon 1987. J. Mar. Res. 48, 359-378.

Urick, R.J., 1983. Principles of Underwater Sound. 3rd ed., McGraw-Hill, New York, 423pp.

Veerayya, M., Karisiddaiah, S.M., Vora, K.H., Wagle, B.G., Almeida, F., 1998. Detection of gas-charged sediments and gas hydrate horizons along the western continental margin of India. Geol. Soc. London, Special Publications 137, 239-253.

Veerayya, M., Wagle, B.G., Vora, K.H., Karisiddaiah, S.M., Almeida, F., 1991. Geomorphology and shallow structure of the western continental margin of India, Int. Symp. Oceanography of the Indian Ocean. Natl. Inst. Oceanogr. Goa, India p. 55 (Abstr.).

Wen, R., Larsen, R.S., 1996. Mapping oil seeps on the seafloor by Gloria Side-Scan Sonar Images- A case study from the Northern Gulf of Mexico. Nonrenew. Resour. 5, 141-154.

Yun, J.W., Orange, D.L., Field, M.E., 1999. Subsurface gas offshore of northern California and its link to submarine geomorphology. Mar. Geol. 154, 357-368.

Figure captions

Fig. 1: (a) Location of study area including some of the main structural features (from Mukhopadhyay et al., 2008) of the region. On land Dharwarian trend shown as dotted lines is well-established NNW-SSE trending Precambrian orogenic structure. Red highlighted lines and grey shade indicate the identified bottom simulating reflectors (Drawn after Rao et al., 2001). MSBR refers to Mid-Shelf Basement Ridge, and WCF indicate West Coast Fault. (b) Backscatter map of the study area showing 160 to 320m isobath with an interval of 20 m depth. Pockmarks are indicated by crossed circles. Black, blue and red circles with cross marking represent circular, elliptical and elongated pockmarks, respectively. Dashed lines indicate location of identified faults. Black arrows showing bottom current directions. Solid black lines represent location of the corresponding profiles for Figures 4a-c, 6 and 7. Inset shows outline map of western continental margin of India with the location of the part of the Arabian Sea.

(Approximate location: section 1)

Fig. 2: Histograms of morphological characteristics (a) length, (b) width, (c) relief, (d) perimeter distance, (e) aspect ratio (length/width) and (f) average slope angle of pockmark's sidewall.

(Approximate location: sub-section 4.1)

Fig. 3: Perspective view of bathymetry of typical pockmarks that are (a) circular, (b) elliptical, (c) elongated, (d) composite and (e) and (f) forming chain (scale is approximate; contour interval 0.5 m).

(Approximate location: sub-section 4.1)

Fig. 4: Backscatter strength and bathymetric profiles for three locations and adjacent areas are shown. Stronger backscatter strength from the centres and upper sidewalls of pockmarks are distinctly indicated. Locations of these profiles are also marked in Fig. 1b.

(Approximate location: sub-section 4.1)

Fig. 5: (a) Rose diagram showing pockmark orientations (defined by their major axis). (b) Composite bar graph showing orientations of circular, elliptical and elongated pockmarks. (c) Histogram of pockmark distribution. (d) Scatter diagram of backscatter strengths at pockmark centre and different water depth.

(Approximate location: sub-section 4.1)

Fig. 6: (a) 3D multibeam bathymetric map of the study area showing faults and pockmarks. Pockmarks are mainly concentrated along fault axis. Lines A-B and SW-NE show the locations of sections drawn in figs 6b and 7a-d respectively. (b) Single-beam echo-sounder (frequency: 33 kHz) section (line A-B), showing pockmark, faults, seeps, and terrace like feature.

(Approximate location: sub-section 4.1)

Fig. 7: A composite figure showing SW-NE trending sections/profiles corresponding to (a) single channel 4.5 kJ sparker, (b) 3.5 kHz sub-bottom profiler, (c) multibeam bathymetry and (d) backscatter data. P- pockmarks, F- faults, m- multiple reflectors, Bp- buried pockmark. The profile location is marked in Figs. 1b and 6a. Scale of x-axes is constant for a-d, whereas scale of y-axes is varying for a-c.

(Approximate location: sub-section 4.1)

Fig. 8: Histogram showing bimodal pockmarks distribution from the central fault (located in Figure 1b) in two distinct deep and shallow regions.

(Approximate location: sub-section 5.2.2)

Fig. 9: Correlation diagrams of various parameters with pockmark relief. Lines and associated dotted lines show the regressions along with their 95% confidence limits. Moderate to strong correlations are observed with pockmark (a) slope angles, (b) length, (c) width, and (d) perimeter distance. Crossed circle and filled circle denotes shallow area (<210 m) and deep area (>210 m) respectively.

(Approximate location: sub-section 5.2.3)

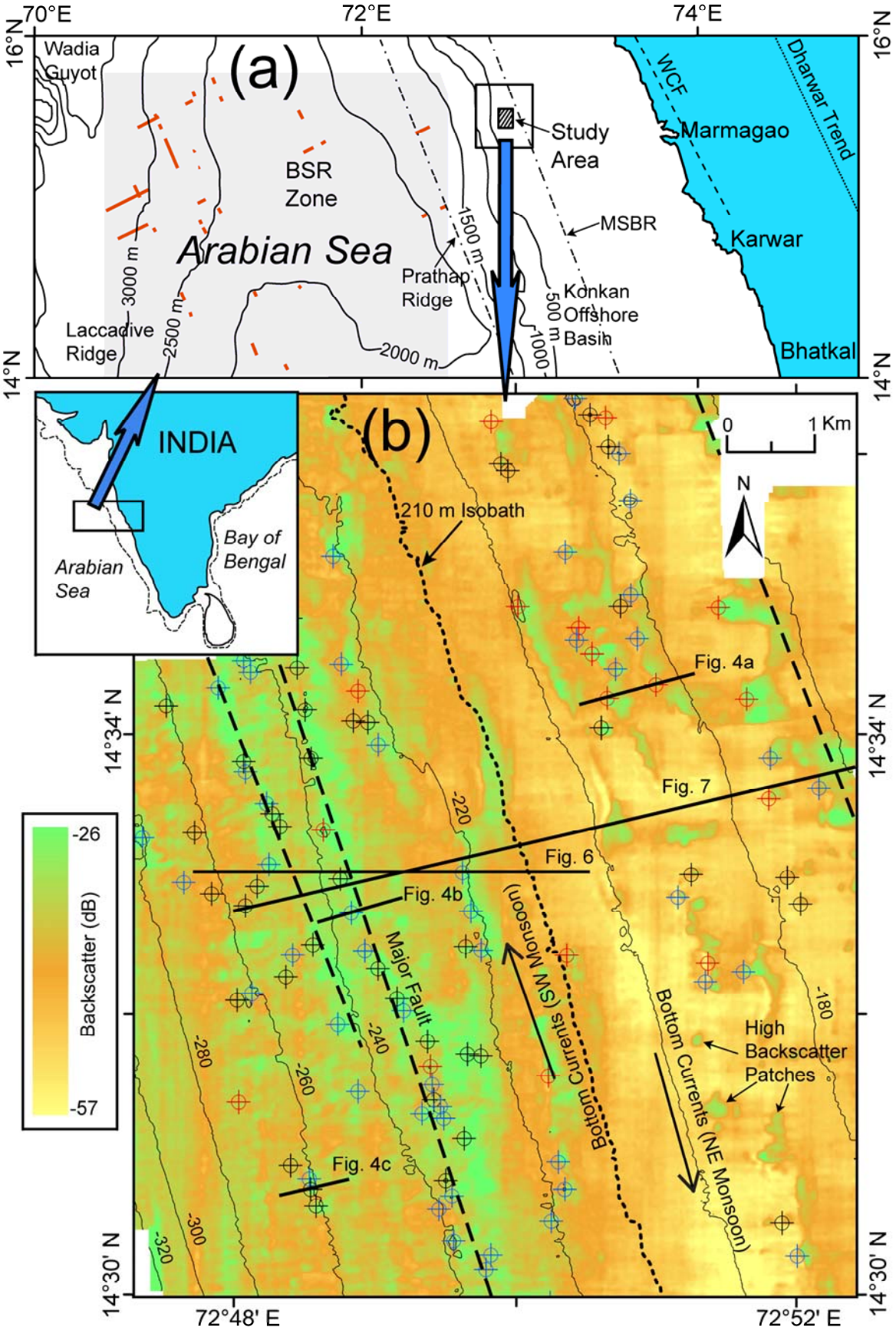
70°E
72°E
74°E
16°N
14°N
(a)
Wadia Guyot
BSR Zone
Arabian Sea
Laccadive Ridge
3000 m
2500 m
2000 m
1500 m
1000 m
500 m
Prathap Ridge
Study Area
MSBR
Konkan Offshore Basin
WCF
Dharwar Trend
Marmagao
Karwar
Bhatkal
INDIA
Bay of Bengal
Arabian Sea
(b)
0
1 Km
N
210 m Isobath
Fig. 4a
Fig. 7
Fig. 6
Fig. 4b
Fig. 4c
Major Fault
Bottom Currents (SW Monsoon)
Bottom Currents (NE Monsoon)
High Backscatter Patches
-220
-240
-260
-280
-300
-320
-180
-26
-57
Backscatter (dB)
14°34' N
14°30' N
72°48' E
72°52' E

Fig. 1

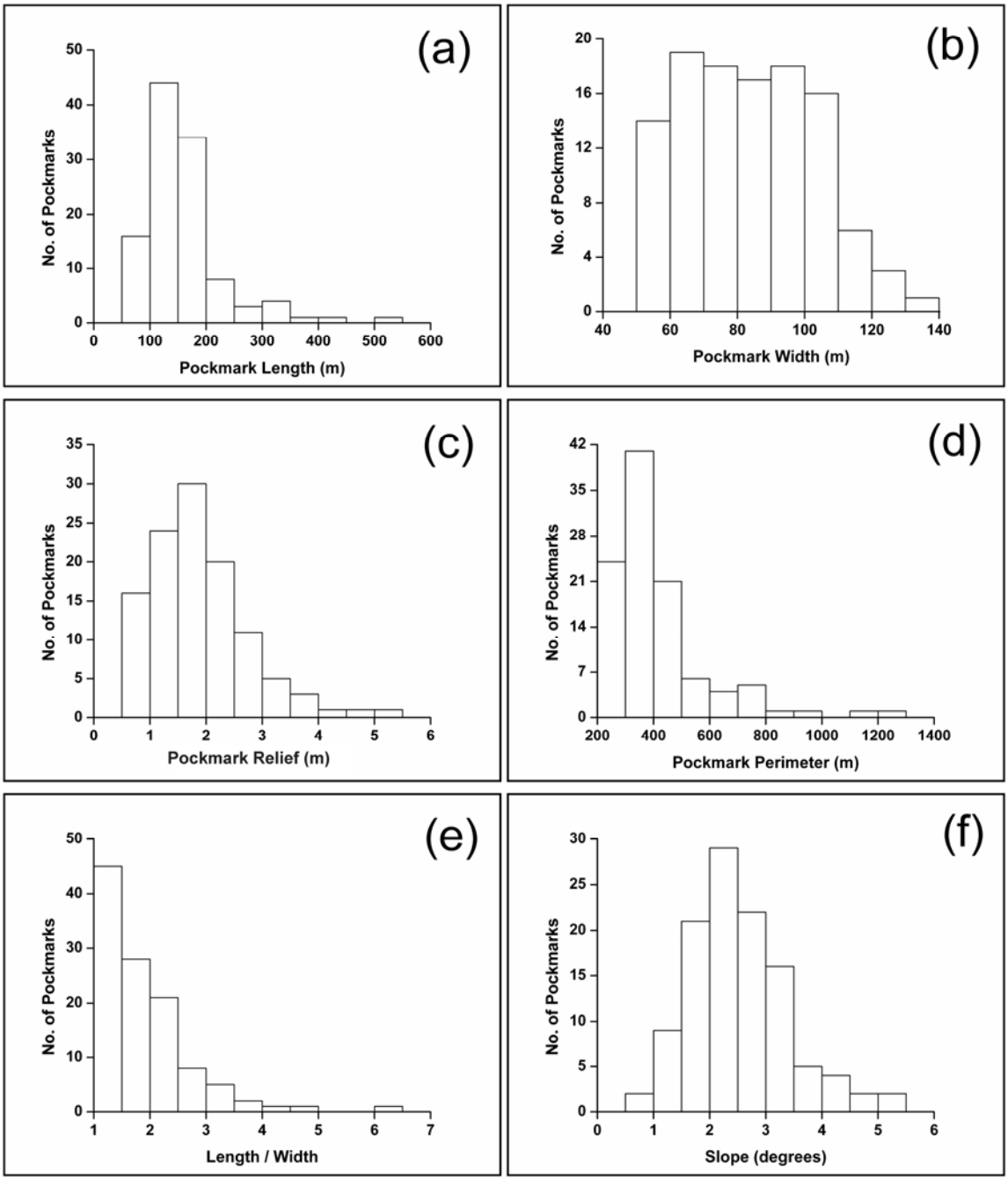
(a)
No. of Pockmarks
Pockmark Length (m)
(b)
No. of Pockmarks
Pockmark Width (m)
(c)
No. of Pockmarks
Pockmark Relief (m)
(d)
No. of Pockmarks
Pockmark Perimeter (m)
(e)
No. of Pockmarks
Length / Width
(f)
No. of Pockmarks
Slope (degrees)

Fig. 2

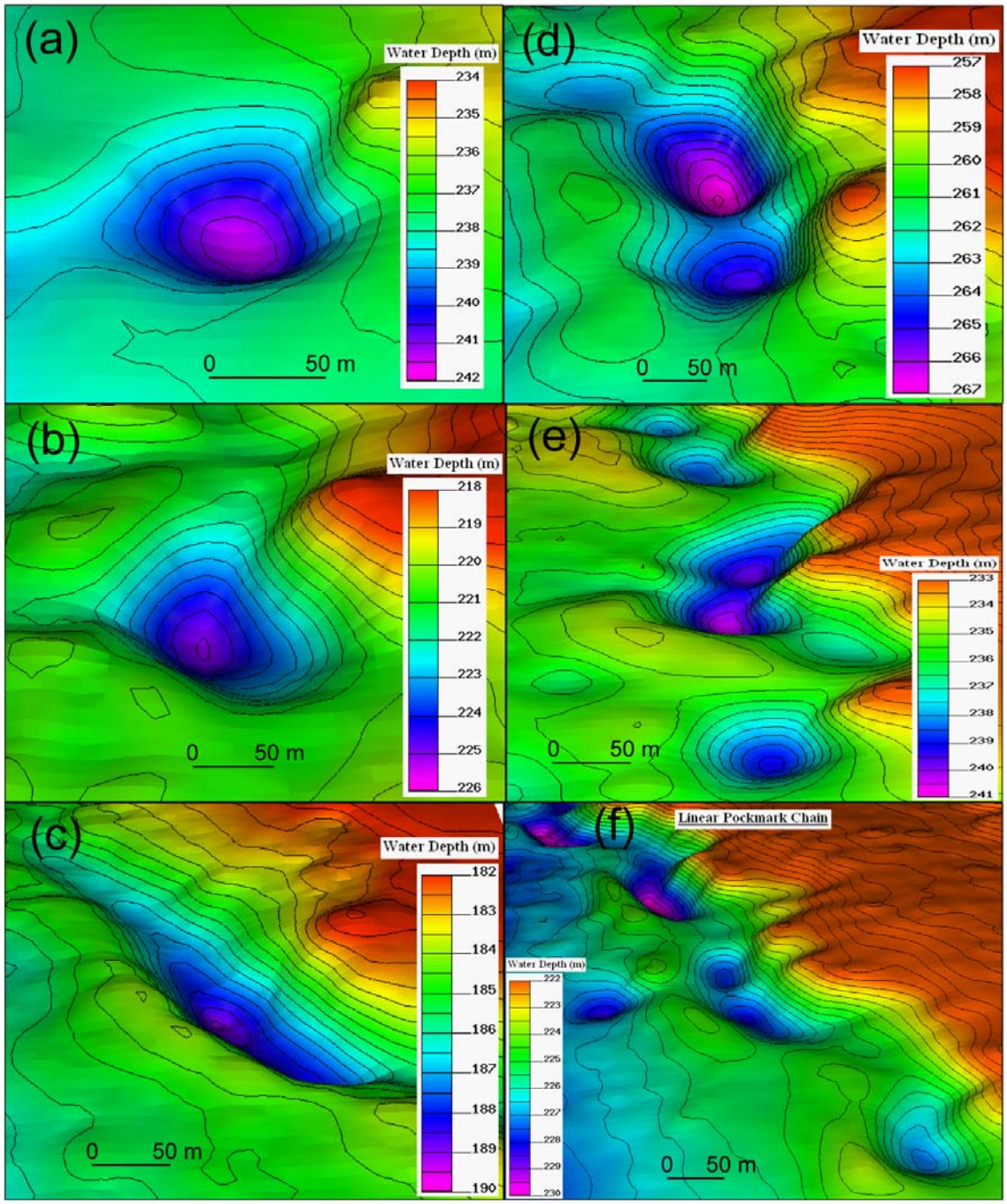
(a)
Water Depth (m)
234
235
236
237
238
239
240
241
242
0
50 m
(d)
Water Depth (m)
257
258
259
260
261
262
263
264
265
266
267
0
50 m
(b)
Water Depth (m)
218
219
220
221
222
223
224
225
226
0
50 m
(e)
Water Depth (m)
233
234
235
236
237
238
239
240
241
0
50 m
(c)
Water Depth (m)
182
183
184
185
186
187
188
189
190
0
50 m
(f)
Linear Pockmark Chain
Water Depth (m)
222
223
224
225
226
227
228
229
230
0
50 m

Fig. 3

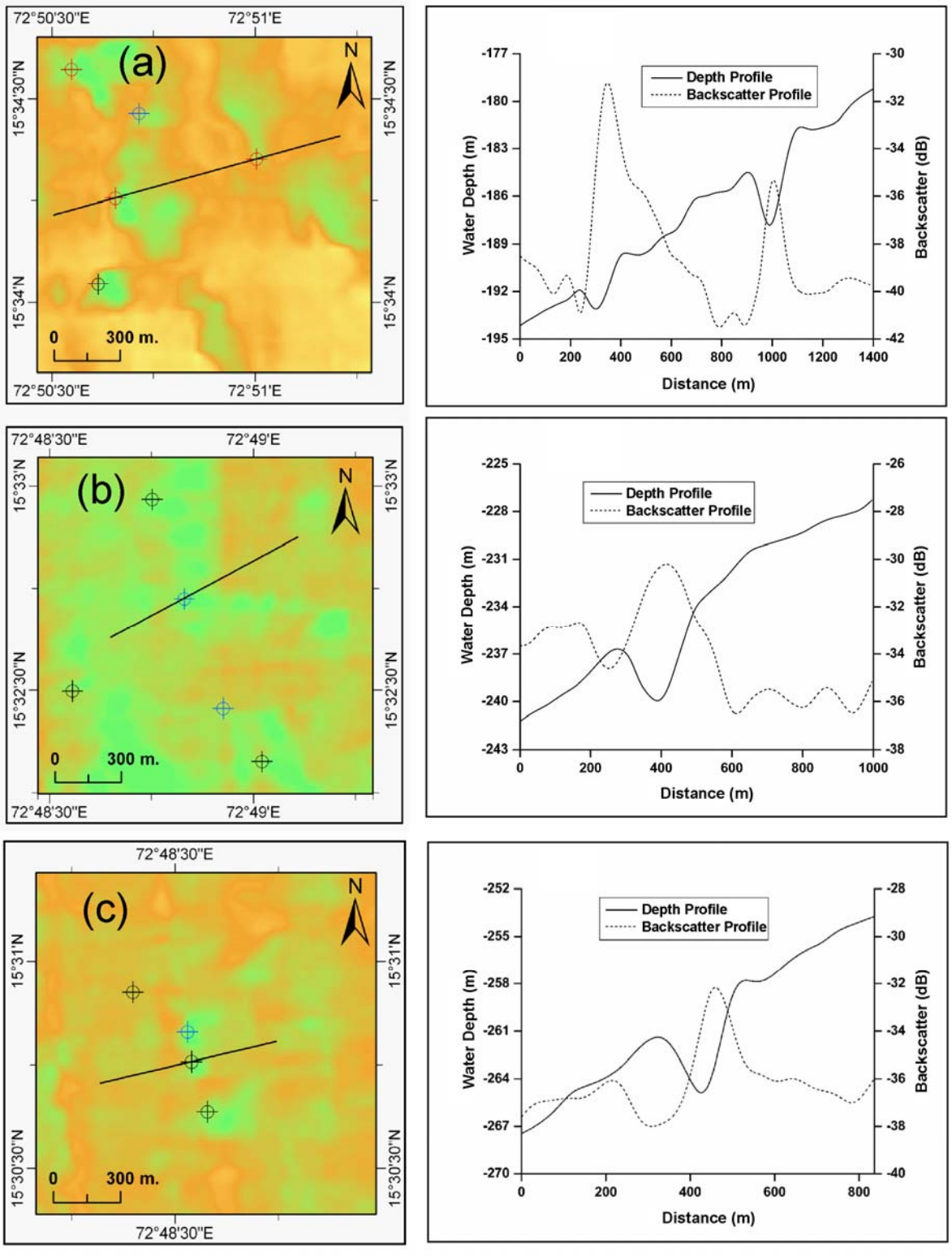
72°50'30"E
72°51'E
(a)
N
15°34'30"N
15°34'N
0
300 m.
Depth Profile
Backscatter Profile
Water Depth (m)
Backscatter (dB)
Distance (m)
72°48'30"E
72°49'E
(b)
15°33'N
15°32'30"N
72°48'30"E
72°49'E
(c)
15°31'N
15°30'30"N
72°48'30"E

Fig. 4

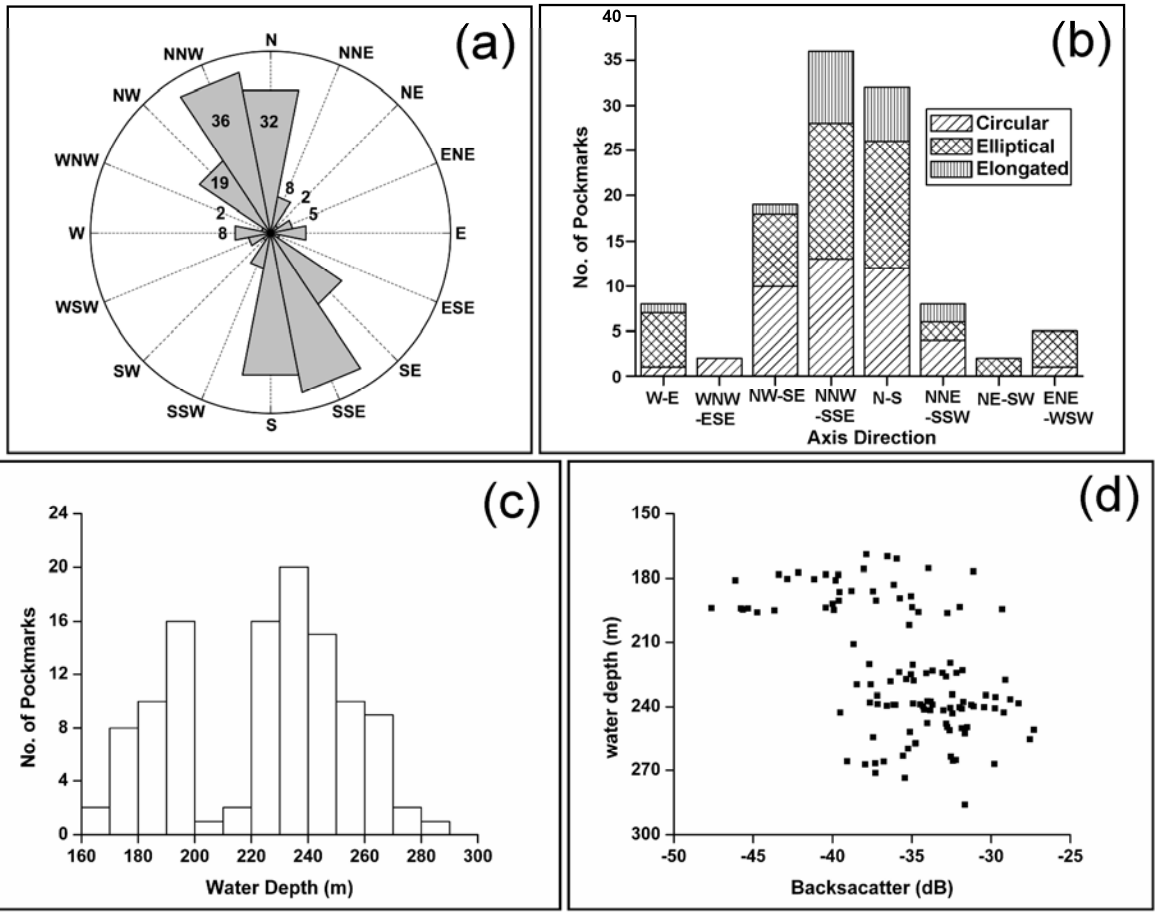
(a)
N
NNE
NE
ENE
E
ESE
SE
SSE
S
SSW
SW
WSW
W
WNW
NW
NNW
36
32
19
8
2
5
2
8
(b)
No. of Pockmarks
Circular
Elliptical
Elongated
W-E
WNW -ESE
NW-SE
NNW -SSE
N-S
NNE -SSW
NE-SW
ENE -WSW
Axis Direction
(c)
No. of Pockmarks
Water Depth (m)
(d)
water depth (m)
Backsacatter (dB)

Fig. 5

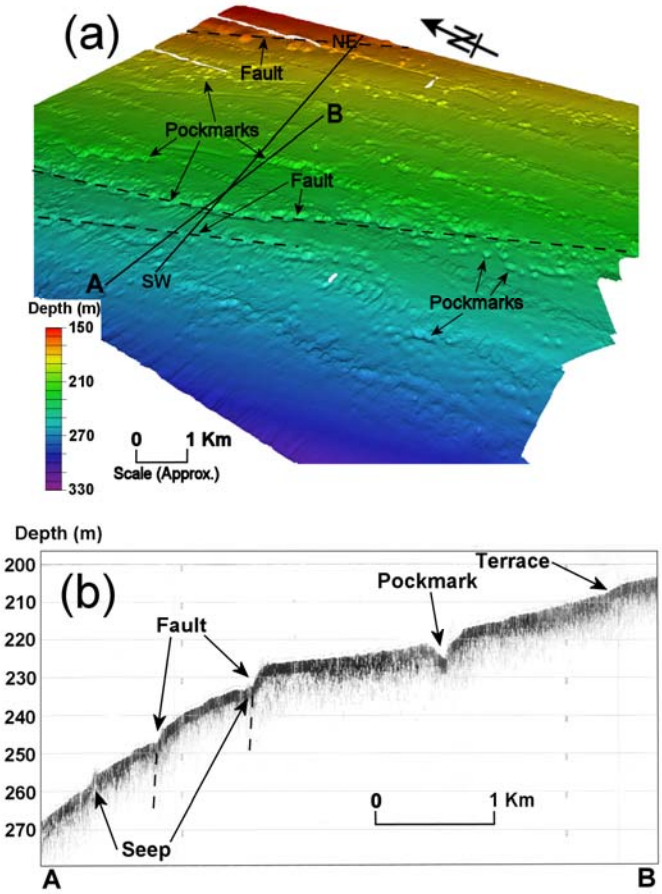
(a)
NE
Fault
B
Pockmarks
Fault
A
SW
Pockmarks
Depth (m)
150
210
270
330
0
1 Km
Scale (Approx.)
Depth (m)
200
210
220
230
240
250
260
270
(b)
Terrace
Pockmark
Fault
0
1 Km
Seep
A
B

Fig. 6

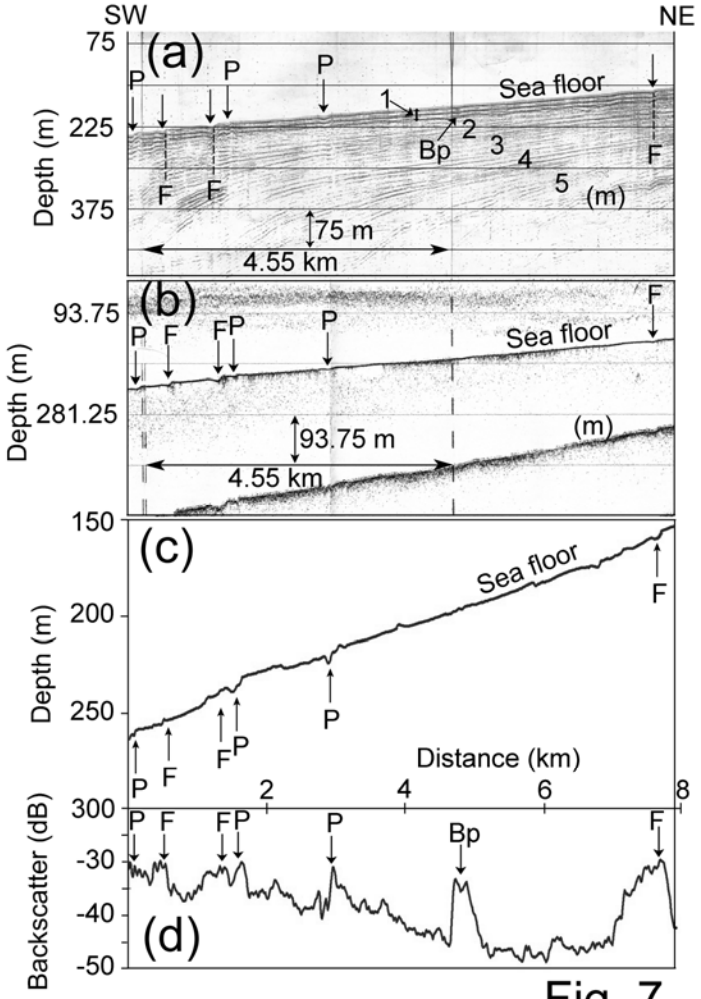
SW
NE
(a)
75
225
375
Depth (m)
P
F
Sea floor
1
2
3
4
5
Bp
(m)
75 m
4.55 km
(b)
93.75
281.25
93.75 m
4.55 km
(c)
150
200
250
Distance (km)
2
4
6
8
(d)
300
-30
-40
-50
Backscatter (dB)

Fig. 7

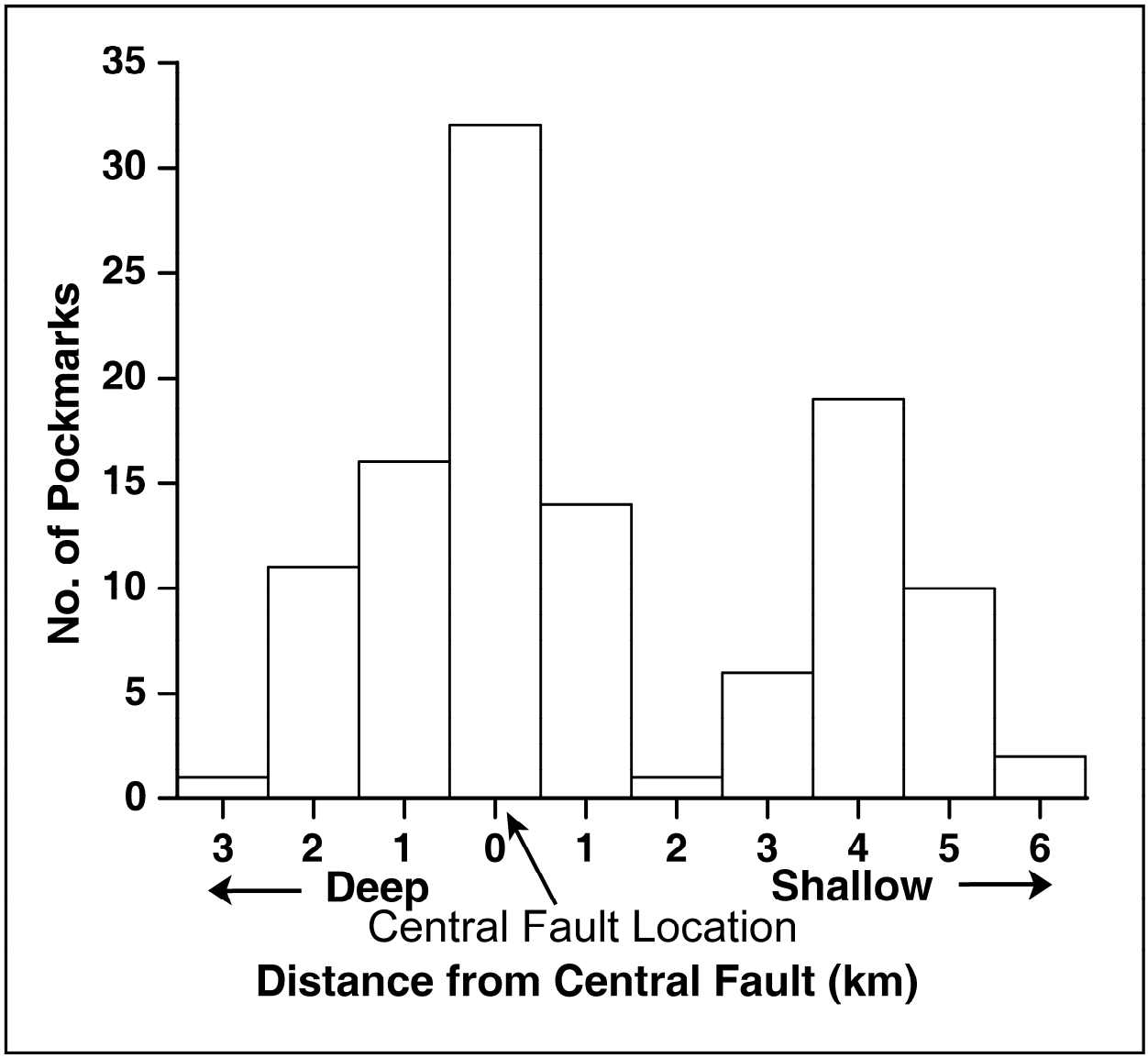
35
30
25
20
15
10
5
0
No. of Pockmarks
3
2
1
0
1
2
3
4
5
6
Deep
Shallow
Central Fault Location
Distance from Central Fault (km)

Fig. 8

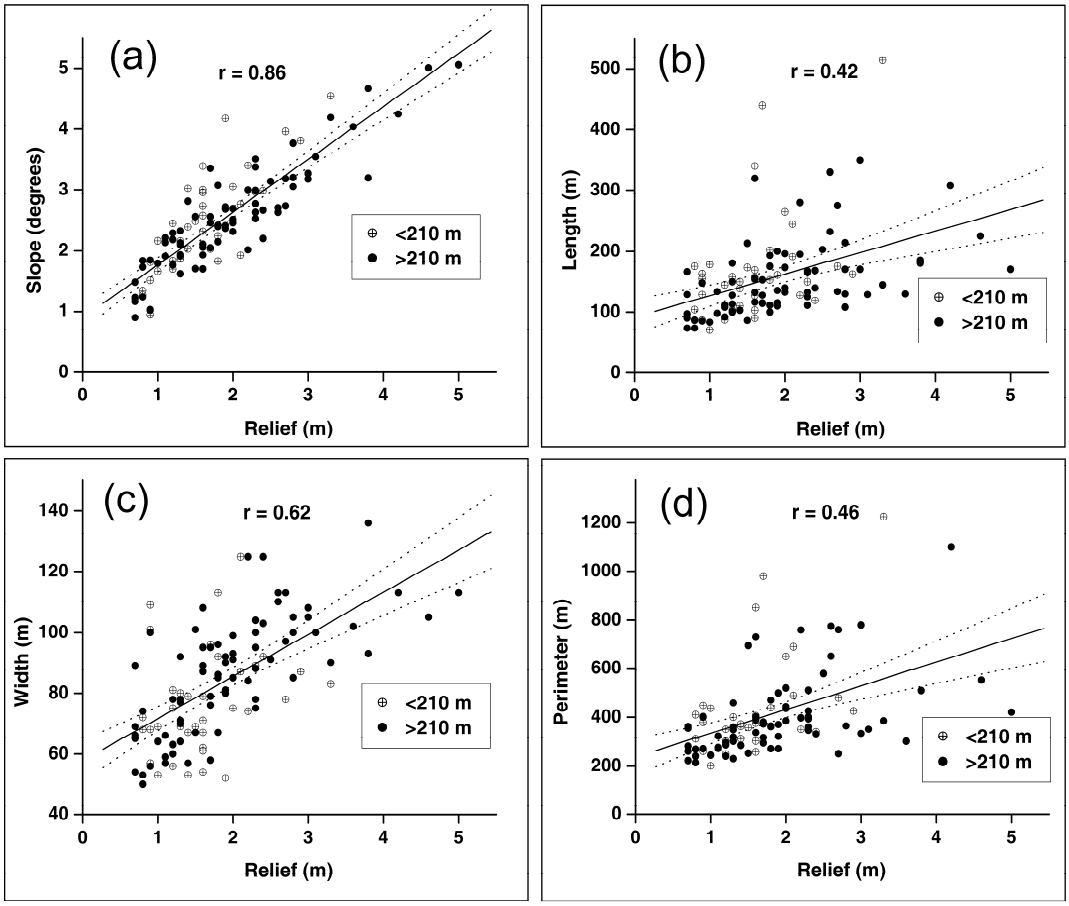
(a)
r = 0.86
Slope (degrees)
Relief (m)
<210 m
>210 m
(b)
r = 0.42
Length (m)
Relief (m)
<210 m
>210 m
(c)
r = 0.62
Width (m)
Relief (m)
<210 m
>210 m
(d)
r = 0.46
Perimeter (m)
Relief (m)
<210 m
>210 m

Fig. 9